Hindawi
Advances in Polymer Technology
Volume 2023, Article ID 7343194, 16 pages
https://doi.org/10.1155/2023/7343194

Research Article

Tailoring the Curing Kinetics of NBR-Based Rubber Compounds for Additive Manufacturing of Rod Seals

Lion Sundermann,[1] **Sebastian Leineweber**,[2] **Benjamin Klie**,[1] **Heike Wittek**,[1] **Thomas Ebel**,[3] **Birger Reitz**,[2] **Kathrin Ottink**,[3] **Matthias Graf**,[3] **Tobias Lankenau**,[3] **Ludger Overmeyer**,[2] **and Ulrich Giese**[1]

[1]*Deutsches Institut fuer Kautschuktechnologie e.V., Hanover, Germany*
[2]*Institut fuer Transport und Automatisierungstechnik, Leibniz Universitaet Hannover, Hanover, Germany*
[3]*Hochschule Emden/Leer, Emden, Germany*

Correspondence should be addressed to Benjamin Klie; benjamin.klie@dikautschuk.de

Received 7 February 2023; Revised 19 June 2023; Accepted 4 July 2023; Published 22 August 2023

Academic Editor: Pierre Verge

The additive manufacturing (AM) of elastomeric parts based on high-viscosity reinforced rubbers has increasingly become a topic of scientific research in recent years. In addition to the viscosity, which is several decades higher during processing than the viscosities of thermoplastics, the flowability of the compound after the printing process and the necessary chemical crosslinking of the printed component play a decisive role in producing an elastic, high-quality, and geometrically stable part. After the first technological achievements using the so-called additive manufacturing of elastomers (AME) process, the knowledge gained has to be transferred first to concrete industrial parts. Therefore, in this study, the cure kinetics of a conventional rubber compound are tailored to match the specific requirements for scorch safety in the additive manufacturing of an industrial 2-component rod seal based on an acrylonitrile butadiene rubber O-ring in combination with a thermoplastic polyurethane as the base body. Experimental tests on a test rig for rod seals demonstrate the functionality of this additively manufactured 2-component rod seal.

1. Introduction

For a long time, additive manufacturing of materials with elastomeric properties was limited to silicone rubbers and block copolymers with rubber-elastic properties, also known as thermoplastic elastomers (TPEs) [1, 2]. More recently, our preliminary work [3–6] and the research results of Drossel et al. [7, 8] have shown that carbon black-filled rubber-based elastomers can also be processed additively, which makes this technology interesting for the production of prototypes, spare parts, and highly individualized products [9]. In addition to the high viscosity of rubber compounds (especially during processing) compared to that of thermoplastic materials, the two-step production process makes the additive manufacturing of rubber components particularly challenging. In the first step, the component is additively manufactured, and in the second step, the necessary vulcanization in an oven takes place, which gives the component its dimensional stability and its rubber-elastic properties [10].

Another significant challenge is that a homogeneous vulcanization is highly time-, temperature- and geometry-dependent. One limiting factor is the thermal conductivity of the compound. The vulcanization time must be determined individually for each component depending on the vulcanization temperature, compound recipe, and corresponding curing kinetics. Manufacturing fine structures makes it even more difficult to find a unified vulcanization time for the whole component. A circumstance in which thinner structures are not already over-vulcanized and larger volumes are not completely vulcanized yet at the end of the cycle time must be avoided. Therefore, the optimum vulcanization time must be identified before the actual process starts. This is determined in the following with a heat transfer simulation in an oven and mixture-specific crosslinking isotherms, measured by rheometry.

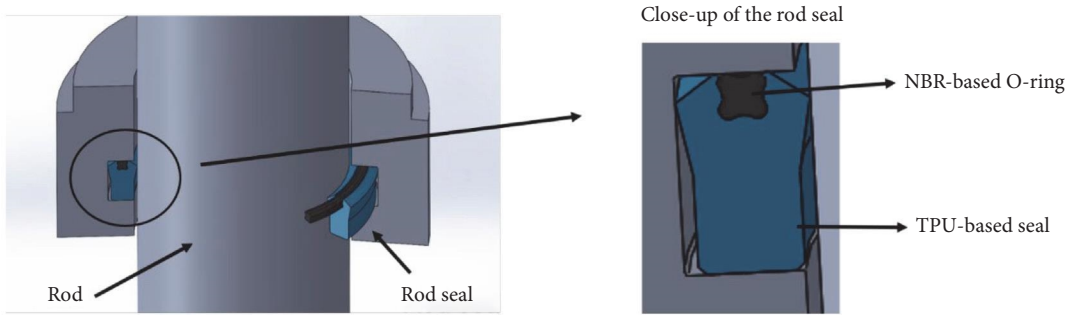

Figure 1: Functional principle of a 2 K rod seal consisting of a TPU and NBR-based material.

A steep ascent in the vulcanization curve is necessary to reduce dimensional deviation during the vulcanization process due to the flow behavior of the rubber material when no surrounding shell structure is printed to stabilize the compound geometrically. Fast cure rates can be obtained by using ultra-fast accelerators or accelerator combinations based on thiuram derivates. When two component (2 K) parts of rubber and thermoplastics should be printed, scorching can be a significant problem due to the extended dwell time for the second component during the processing of the first. In this work, the manufacturing of a rod seal demonstrates the challenges in the 3D printing of components consisting of rubber and thermoplastics.

The operating principle of the seal is explained in Figure 1 using the reference seal (*AB SKF*, PTB series) as an example.

The seal itself consists of a thermoplastic polyurethane (TPU)-based material manufactured typically by injection molding, which has direct contact with the metal rod and ensures leak tightness. An NBR-based rubber O-ring is combined with the TPU seal to enhance and ensure the radial force on the rod during operation. In additive manufacturing, the first layers only consist of TPU, while the rubber mixture is already inside the heated extruder and ready to print. Fast vulcanization kinetics could cause scorched material during AM before passing the nozzle, which might reduce layer-to-layer bonding due to the reduced flow of the material. In addition, a decreased throughput in the process could occur and lead to inhomogeneities within the printed part. In the case of strong scorching in the extruder, mechanical components such as screws, the extruder drive, or gears can be damaged. When both materials have to be within a single layer, the TPU is first printed to support the dimensional stability of the rubber mixture by acting as a shell-like structure. The printing of both materials then alternates until the last layer. A decreased temperature in the extrusion process extends the scorch period but also increases the viscosity of the mixture. Since the miniature extruder used in this study (Type *ZE9* from *Three-Tec GmbH*) suffers from a lack of torque, a higher temperature is beneficial to reduce the mixture viscosity of compounds filled with high amounts of carbon black. Furthermore, a lower viscosity in the printing process can improve the layer–layer bonding and thus the isotropy of the part. Therefore, a combination of scorch safety during the entire additive manufacturing and fast-curing kinetics in the subsequent vulcanization in the oven is fundamental to mixture development in rubber 3D printing. Using the present setup of the 3D printer, it is not yet possible to manufacture TPU and rubber components in a serial process. The installed printhead is only suitable for the additive manufacturing of thermoplastics, not TPUs. In addition, the adhesion of NBR rubber on the TPU part and heat transfer between both materials before manufacturing the 2K part with one printer are still challenging. In this work, the TPU part was printed with an external TPU printer (*Prusa* i3Mk3S+) to determine a reasonable printing time for it [11]. A compromise between rapid printing to reduce the scorching risk and the adequate quality of the part has to be found. Furthermore, the weight of the rubber extruder causes strong vibrations when a printing velocity of more than 40 $mm \cdot s^{-1}$ is used.

Through the use of delayed-action sulfenamide derivates [12] as binary accelerators in combination with thiuram systems, the induction period can be adjusted by varying the ratio [13]. The crosslinks created in sulfur vulcanization can be characterized as mono-, di-, and polysulfidic and can be in isolated or vicinal locations [14]. Changes in the ratio of sulfur/accelerator lead to different crosslink structures. While a decreased amount of accelerator leads to more polysulfide bonds, the reduction of sulfur increases the number of mono- and disulfide bonds [15]. That influences mechanical properties and thermal resistance, and application-specific validation tests can be required. Within the same chemical class of accelerators, there are differences in their effect on curing kinetics. Sulfenamides' steric hinderances of the molecules also reduce the cure rate and may extend the scorch delay, depending on the rubber type [16]. To enhance scorch safety without changing the present cure system, a so-called pre-vulcanization inhibitor (PVI) can be used to extend the induction period. In the industry, N-cyclohexylthiophthalimide (CTP) is most commonly used [17], which was patented in 1970 by Coran et al. [18]. In sulfenamide-based crosslinking systems, the scorch time is extended by CTP molecules reacting with the typical intermediate mercaptobenzothiazole (MBT) to create 2-cyclohexyldithiobenzothiazole (CDB) [19] before forming crosslinking precursors with sulfur and thioles from accelerator molecules [20]. Subsequently, CDB takes part in the crosslinking as a delayed action accelerator with a lower cure rate [21]. However, concentrations of more than 0.5 phr CTP may lower the cure density, and thus mechanical properties can be reduced [22]. In the case of rod seals, a lower crosslink density would lead to a

Table 1: Reference recipe #1 and final recipes after optimization.

Ingredients	#1 Reference recipe (phr)	#2 Simply adopted recipe with CTP (phr)	#3 Fundamentally optimized recipe (phr)
NBR (Krynac 3330 F)	100	100	100
Carbon black (N772)	100	100	100
Plasticizer (Struktol TS 35)	5	5	5
Activator (ZnO)	3	3	3
Activator (Stearic acid)	0	0	1
Antioxidant (6PPD)[a]	2	2	2
Antioxidant (TMQ)[b]	1	1	1
Processing aid (Struktol WB222)	1.5	1.5	1.5
Accelerator (TBzTD)[c]	3	3	3
Sulfur donor (CLD[d] GR80)	1	1	0
Accelerator (MBTS)[e]	1.5	1.5	0
Sulfur preparation (Struktol SU 105)	1.6	1.6	1.6
Accelerator (DCBS)[f]	–	–	**2**
Retarder (CTP)[g]	–	**1**	**0.25**

[a]6PPD, N-(1,3-Dimethylbutyl)-N'-phenyl-pphenylenediamine; [b]TMQ, 2,2,4-trimethyl-1,2-dihydroquinoline; [c]TBzTD, Tetrabenzylthiuram disulfide; [d]CLD, Caprolactam disulfide; [e]MBTS, Dibenzothiazyl disulfide; [f]DCBS, N,N-Dicyclohexyl-2-Benzothiazole sulfenamide; [g]CTP, N-cyclohexylthiophthalimide.

lower modulus of elasticity at small elongations as well as a higher compression set. Thus, the radial force applied to the rod after the assembly would be reduced, and the tightness might be negatively affected.

Curing kinetics and crosslink density and structure are also influenced by the concentration of sulfur, type of activators, and their ratio. The most widely used activator in the rubber industry is zinc oxide (ZnO) [23]. Due to its hydrophilic character and thus low solubility, high amounts are added to the mostly nonpolar rubber polymers. The solubility can be increased by fatty acids such as stearic acid, which facilitate the formation of an accelerator-zinc stearate complex as an intermediate in the crosslinking mechanism [24–26]. Together with the amine fragment from sulfenamide accelerators, the carboxylate of stearic acid stabilizes as a ligand [27].

Starting from an adopted industrial NBR-based fuel seal recipe, two different approaches to tailoring the vulcanization kinetics to obtain an industrial 3D-printable compound are presented in this work. Considering the limiting process parameters such as printing speed and resolution, the kinetics were optimized in the following ways: First, additional CTP was used in different concentrations to extend the induction period of the material. In a second approach, a new curing system was tailored to achieve superior mechanical properties and a higher degree of crosslinking compared to the use of CTP with comparable retardation. To validate the adopted mixtures, their resulting curing kinetics, crosslink density, and mechanical behavior are characterized below.

2. Materials and Methods

2.1. Rubber Recipes. The rubber formularies were based on a typical fuel-resistant seal recipe. NBR rubber (Krynac 3330 F) with an acrylonitrile content of 33% and a Mooney viscosity at 100°C of 30 MU, carbon black (N-772) with a STSA of 30 m^2/g and an OAN of 65 ml/100 g, antioxidants (6PPD, TMQ), activators (ZnO, stearic acid), and a plasticizer (Struktol WB222) were used. The crosslinking was carried out with a sulfur-based vulcanization system with a fixed concentration of a 50% sulfur preparation (Struktol SU105), variable accelerators (TBzTD, MBTS, CBS, DCBS), and a sulfur donor (CLD). The most beneficial mixtures (#2 and #3) are compared with the reference compound #1 in Table 1.

2.2. Sample Preparation. The rubber mixtures were produced using an industrial internal 5 l mixer (*Werner & Pfleiderer* GK 5E) with intermeshing rotors and a feeding volume of 70% at 40°C and 40 rpm. The polymer was plasticized for 1 min before carbon black was added and mixed for 1 min until the torque level lowered to a constant one. The additives were incorporated for 1 min as well. The mixture obtained was cooled down for 5 min on a two-roll mill, and rubber sheets were produced for further processing steps. The crosslinking components were added on a double-roll mill for 8 min at 50°C. The rotational speeds used were 10 and 12 min^{-1} for the first and second rollers, respectively. The nip was 1.5 mm. Additive-manufactured samples were vulcanized without pressure in a laboratory oven at 160°C, with their respective vulcanization times set according to the precomputed curing time t_{90}. Reference vulcanizates of 2 mm thickness were produced in a conventional heating press at 160°C and $2.8 \cdot 10^7$ Pa. Due to the limitation of the size of the internal mixer and thus the batch weight, more than one batch had to be produced to provide a sufficient amount of material for the characterization and additive manufacturing. Therefore, due to the individual mixing process, the numerical values of the characterization methods for samples from different batches could only be roughly compared due to the individual mixing process. However, the trend within the test series represented the achievement of both optimization

Table 2: Usage of the mixed compound with the corresponding batch number.

Usage and characterization method	Batch
Simulation of vulcanization in a heated oven	1
Optimization series with CTP: Rheometry, infrared spectroscopy, light microscopy, tensile tests (conventional manufactured in heat press), awelling, RPA, Mooney Scorch	2
Optimization series with exchanged cure system: Rheometry, tensile tests (conventional manufactured in heat press and additively manufactured), RPA	3
Swelling, Mooney Scorch, 3D printing of rubber O-ring	4

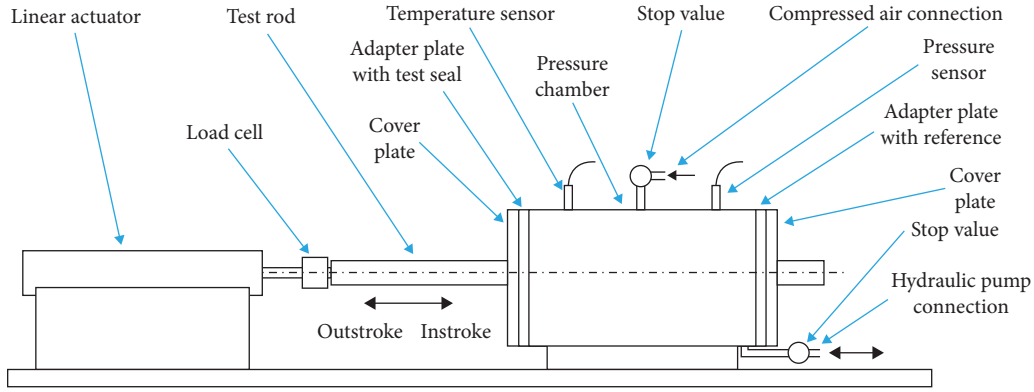

Figure 2: Schematic layout of the test stand for rod seals at the University of Applied Sciences in Emden.

approaches. In Table 2, the number of a batch is assigned to the individual purpose of the mixture.

2.3. Additive Manufacturing. The 3D printer was a former CNC milling machine that was converted to a fused filament fabrication printer for additive manufacturing of elastomers. Technical details can be deduced from former publications [3, 4]. A nozzle diameter of 0.6 mm was used for all printing experiments. As a compromise concerning viscosity reduction and scorch safety, the temperature was enhanced in the three heating zones (Off/70°C/100°C). The travel speed during the printing process was 10 mm·s^{-1}. To achieve improved adhesion between the print bed and the first printed rubber layer, the carbon printing plate used was coated with a commercially available printing glue spray (*Weicon*® Adhesive Spray detachable). In addition, the rotational speed was adjusted to obtain a slight over-extrusion (13 mm·s^{-1}). Together with the nozzle distance of 0.4 mm from the print bed, this created more pressure and cohesion between the layers. The stripe distance of the 3D-printed samples was 0.8 mm.

2.4. Rheometry. The vulcanization time t_{90} and scorch time t_{10} were determined by a *Monsanto* MDR 2000 E rheometer at 160°C. A rubber process analyzer (RPA *elite* from *TA Instruments*) was used to characterize the kinetics of the vulcanization. The activation energy was calculated based on three isothermal cure curves at temperatures of 140, 160 and 180°C using an Arrhenius approach with a sample size of $n = 1$.

2.5. Infrared Spectroscopy. Infrared Spectroscopy (IR) was carried out by using an Attenuated Total Reflectance-Fourier Transformed Infrared (ATR-FTIR) spectrometer (*Nicolet*™ *iS*™ *50 FT-IR- Spektralphotometer* by *Thermo Fisher Scientific* with an OMNI-Sampler™ unit) in order to collect the spectra in a wavenumber range of 675–4,000 cm^{-1} and a step size of 0.5 cm^{-1}. Transmission spectra with potassium bromide (KBr) as carrier with a weight ratio of 0.49 wt% (Sample/KBR) were carried out with the spectrometer mentioned above, but by using an OMNI-Transmission™ unit in a range of 420–4,000 cm^{-1} and a step size of 2 cm^{-1}.

2.6. Tensile Test. The tensile test of the vulcanizates was carried by means of a *Zwick/Roell* Z010 tensile testing machine according to DIN 53504 and using S2 specimens with a sample size of $n = 5$.

2.7. Dynamic Tests. The dynamic rod seal tests were carried out using the test stand seen in Figure 2 with a sample size of $n = 3$. A linear actuator with a maximum speed of 250 mm·s^{-1} moved a test rod. The test rod slid into two rod seals that sealed a pressure chamber that was filled with hydraulic fluid (mineral oil ISO 32 HM HLP). Consequently, with every movement of the rod, one seal was facing an instroke and the other an outstroke. The reference measurement was done using two conventionally produced rod seals. For the test, an additively manufactured specimen replaced the seal in the left adapter.

The dynamic short-time tests for functionality proof were conducted according to the following schedule: The chamber was filled with hydraulic fluid using a manual pump. After waiting for 10 min, a sequence of 10 in- and outstrokes with 100 mm was performed for the test seal. Another waiting period of 10 min followed. Then the pressure was raised by

1 MPa. The same schedule was repeated until a pressure of 5 MPa was reached.

3. Results and Discussion

3.1. Simulation of the Vulcanization Time

3.1.1. Simulation Procedure to Identify Efficient Vulcanization Times in a Heated Oven. The determination of the optimum vulcanization time was based on a heat transfer simulation for the oven and mixture-specific crosslinking isotherms. The simulation of the vulcanization has been carried out for *the rubber* plates (180 × 80 × 2 mm), which were used for cutting out S2 specimens. The detailed procedure for the simulation can be found in Leineweber et al. [5]. At the beginning, the component was at room temperature, and the forced-air oven was preheated. In preliminary tests, a heat transfer coefficient of 20 $W\cdot(m^2\cdot K)^{-1}$ [28] was validated for the present oven. Similarly, the following guide values were assumed for rubber compounds: a density of 1,200 $kg\cdot m^{-1}$, a specific heat capacity of 1,860 $J\cdot(kg\cdot K)^{-1}$ and a thermal conductivity of 0.26 $W\cdot(m\cdot K)^{-1}$. When the component was placed in the preheated oven, the temperature of the component increases with time. Since the cure time was temperature-dependent, the crosslinking isotherms for the temperatures 120, 130, 140, 150, and 160°C were recorded for an exemplary compound in this case. In Figure 3(a), a cuboid cut open in the center with dimensions of 100 × 20 × 10 mm is exemplarily demonstrated in the simulation setting to better visualize the temperature distribution using a larger specimen. The resulting torque curve according to the simulation is represented in Figure 3(b) and consists of segments of the previous collected curves.

In Figure 3(a), it can be seen that the component heats up from the outside to the inside, as expected. If the component is in the temperature range of 115–125°C, vulcanization is assumed to proceed according to the first isothermal curve (black curve, Figure 3(b)). If the point under observation in the component exceeds the first temperature corridor, the torque achieved so far is determined. The determined torque serves as a starting point on the next highest crosslinking isotherm, which in this case represents the temperature range from 125 to 135°C (red curve, Figure 3(b)). Crosslinking now proceeds according to the curve of these crosslinking isotherms until this temperature corridor is also exceeded. This process continues until the last isotherm (purple curve). The vulcanization is carried out up to vulcanization time t_{90}. This time corresponds to a degree of crosslinking of 90%, which correlates with 90% of the maximum torque absorbed by the crosslinking isotherms. Complete vulcanization then takes place over the cooling time. The temperature distribution in the component allows the degree of vulcanization to be specified on a location-specific basis in the component. Finally, the most stress-critical point in the component should be vulcanized as optimally as possible. In this case, the vulcanization time t_{90} calculated using the simulation tool was 6 min 22 s for NBR-based rubber plates with dimensions of 180 × 80 × 2 mm. The demonstrated approach can be considered a rough first estimate. For optimized results, the specific geometry or curing conditions (oven type, temperature, pressure, material, and surrounding thermoplastic structures for 2 K parts) must be taken into account.

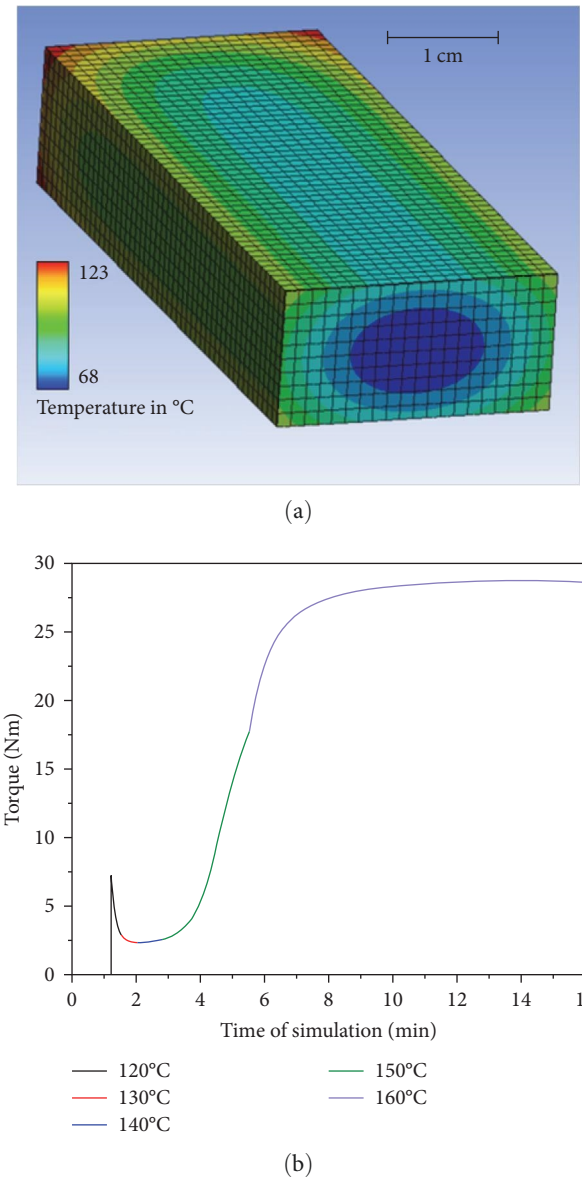

Figure 3: (a) Simulation of heat transfer within a rubber cuboid (100 × 20 × 10 mm); (b) resulting curing isotherm of the simulation of the rubber plates (180 × 80 × 2 mm).

3.1.2. Experimental Validation of the Simulation. Due to the reduced efficiency of heat transfer in the hot air atmosphere in the oven compared to the vulcanization in the heated press, the time for curing was expected to be longer. To determine the optimal vulcanization time, a test series was carried out with non-additive manufactured samples using NBR-based recipe #1. The material was pressed for 10 min at 100°C without any curing activity using a frame of 1.8 mm thickness. The plates were subsequently vulcanized at 160°C in the oven, and time durations varied from 5 to 19 min in 2-min steps. To achieve maximum homogeneous vulcanization, the plate was hung up with metal hooks and placed with

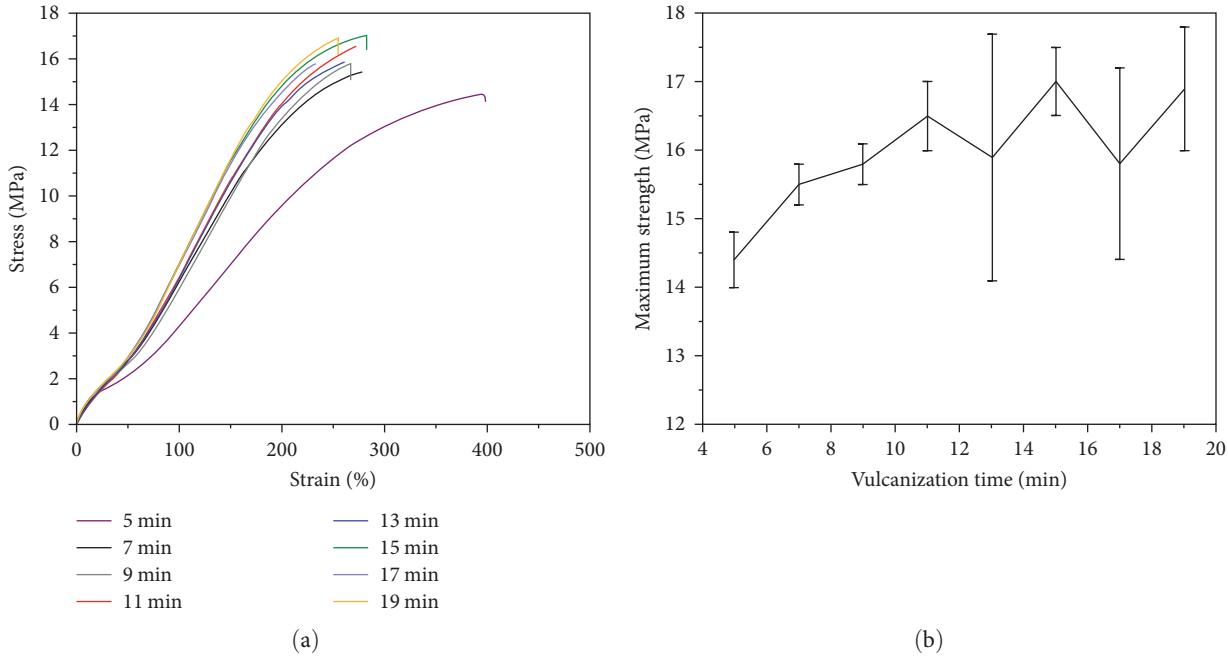

FIGURE 4: Mechanical properties of S2 samples after vulcanization at ambient pressure in an oven heated to 160°C (Batch 1). The data are based on the median values of test series of $n = 5$ each. (a) Stress/strain curves after different vulcanization durations; (b) maximum tensile strength values depending on the vulcanization time.

the 1.8 mm thick side in front of the ventilator so that the air could flow along the sample from both sides. S2 specimens were stomped out of the resulting cured plates, and their tensile properties were tested. The results are shown in Figure 4.

The vulcanization time t_{90} of this NBR-based recipe #1 (Batch 1) at 160°C was determined in the rheometer as 3 min 2 s. In the oven, the 5 min vulcanized sample already showed a steep increase in the stress values after 50% strain, which was typical elastomeric behavior. However, the values of elongation at break were significantly higher and the maximum tensile strength values lower compared to those of samples with longer cure times. It can be assumed that 5 min of cure time in the heated oven obviously leads to an undervulcanized part. From 7 min on, the vulcanization process progressed only slightly, as can be seen in the asymptotical curve of the maximum tensile strength values in Figure 4(b). The optimum vulcanization time was reached at 11 min, because after longer curing, the range of error increased. Since the vulcanization was carried out under atmospheric conditions with oxygen-containing air, the oxidation of the specimen takes place inhomogeneously and starts at the surface of the specimen, which is described by the diffusion limited oxidation (DLO) effect. This increases the number of surface defects and thus the potential for random rupture [29–31]. The simulated duration in the oven was about 5 min shorter than the experimentally determined time, since the opening of the oven door and the associated temperature drop were not considered in the calculation. For NBR-based materials with a thickness of about 2 mm, a general final vulcanization time t_{final} can therefore be assumed to be:

$$t_{\text{final}} = t_{\text{sim}} + 5\,\text{min} \tag{1}$$

when different recipes or batches are produced, the vulcanization time has to be considered individually. To facilitate the determination for vulcanized rubber plates of 2 mm thickness at 160°C, the required time $t_{2\text{mm}}$ can be here given by the temperature difference of about 8 min between the experimental determined optimal vulcanization time in the pressureless oven (11 min) and t_{90} from the rheometer (3 min 22 s):

$$t_{2\text{mm}} = t_{90,160^\circ\text{C}} + 8\,\text{min}. \tag{2}$$

Thus, an entire characterization of the cure behavior at different temperatures can be avoided for new product batches.

3.2. Tailoring of the Vulcanization Kinetics

3.2.1. Vulcanization Kinetics of NBR–Rubber Mixture #1 Extended with CTP. To adjust the kinetics toward a longer scorch time, CTP was used as a retarding agent to elongate the scorch time in the first approach. Different amounts of CTP were mixed while rolling the rubber mixture, and the kinetics of the resulting material were subsequently investigated during the curing process. The rheometer curves are shown in Figure 5.

The curves of Figure 5(a) show a steep ascent in the vulcanization curve for all samples, followed by a plateau and slight reversion. The steep ascent is favorable to retain the dimensional stability in pressureless vulcanization after additive manufacturing. The final values of the torque in the rheometer decreases with an increasing amount of CTP,

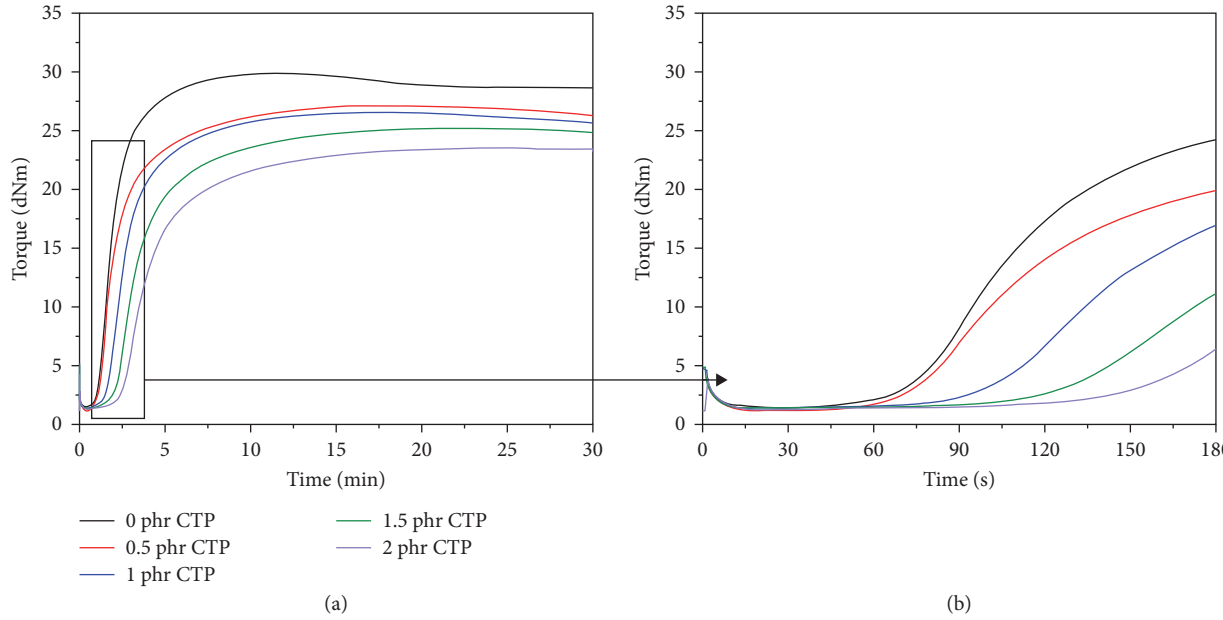

Figure 5: Rheometer curves at 160°C of mixtures containing different amounts of retarding agent CTP in the recipe #1 (Batch 2) and its effect on cure behavior. (a) Rheometer curve; (b) comparison of the induction period in the close-up of (a).

Table 3: Effect of the retarding agent CTP on the vulcanization time t_{90}, scorch time t_{10}, and maximum torque in the rheometer at 160°C.

Amount of CTP (phr)	Vulcanization time t_{90} (s)	Scorch time t_{10} (s)	Maximum torque S´ (dNm)
0 (Ref. #1, Batch 2)	248	76	29.9
0.5	379	77	27.2
1	384	104	26.5
1.5	500	132	25.1
2	559	156	23.5

because the crosslink density decreases with an increasing amount of retarder. From Figure 5(b), it can be deduced that an increasing amount of CTP leads to extended induction periods. While 0.5 phr CTP in the mixture did not show any significant effect on the scorch time, the vulcanization time t_{90} was already extended by 53%. Additionally, the final torque values were lowered significantly without achieving an extended induction period. When 1 phr CTP is used, the scorch time is extended significantly by 37%, and by 105% when 2 phr CTP is used. The vulcanization time t_{90}, the scorch time t_{10} and the numerical values of the maximum torque are presented in Table 3.

The final torque values correspond with the crosslink density of the vulcanized mixture. The lowering effect of CTP on crosslink density can be recognized as the decreased value of the final torque in the rheometer. The numeric values of the crosslink density are later discussed based on the results of swelling experiments. In this case, the torque level of the sample that contained 1 phr CTP was reduced by 11%, the values of the samples with 1.5 and 2 phr were further decreased by 16% and 21%, respectively.

3.2.2. Light Microscopy. The use of 1 phr CTP already showed slight blooming effects after having been stored for two weeks due to insufficient solubility, which dramatically increased when 1.5 phr or more were added, and thus made the sample unusable in further industrial applications. The presence of CTP on the sample surface could be confirmed by light microscopy, which is shown in Figure 6.

When 0.5 phr CTP were added in the mixture, no crystalized CTP could be observed by light microscopy. A CTP content of 1 phr already showed a slight crystallization. The number and size of crystals increased when 1.5 phr CTP was used, and needle-shaped CTP crystals of about 100 μm were present on the surface.

3.2.3. IR-Spectroscopy. ATR-FTIR is commonly used to detect blooming on the surface of rubber substrates caused by curing agents [32]. In this paper measurements have been performed on the surface of the vulcanizates to detect and identify CTP by observing the carbonyl stretches in the phthalimide unit of the molecule. The resulting spectra of different CTP contents in the mixtures and the reference spectrum (KBr) of CTP are shown in Figure 7.

In the ATR-FTIR-spectrum, amounts of 1 phr and more show two characteristic peaks (1,772, 1,734 cm^{-1}) that indicate the C = O stretches [33]. The intensity of the peaks increases when the samples contain more CTP. In this study, the sample based on recipe #2 that contained 1 phr was the most reasonable choice for further tests, because the

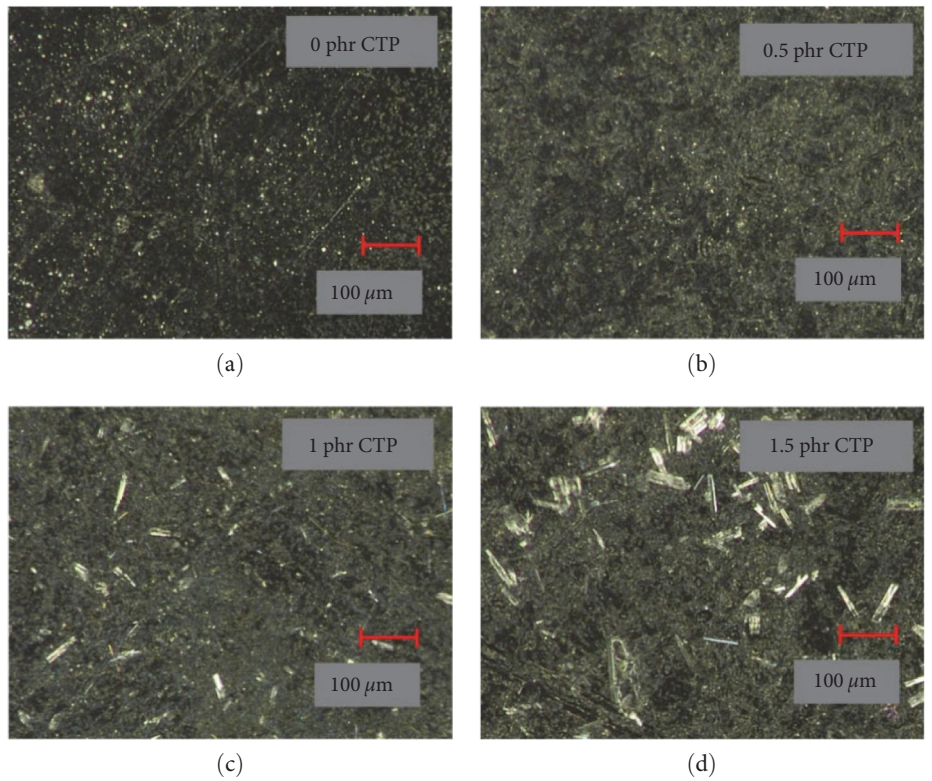

Figure 6: Light microscopy of the surface of vulcanizates with different CTP contents. (a) 0 phr CTP; (b) 0.5 phr CTP; (c) 1 phr CTP and (d) 1.5 phr CTP.

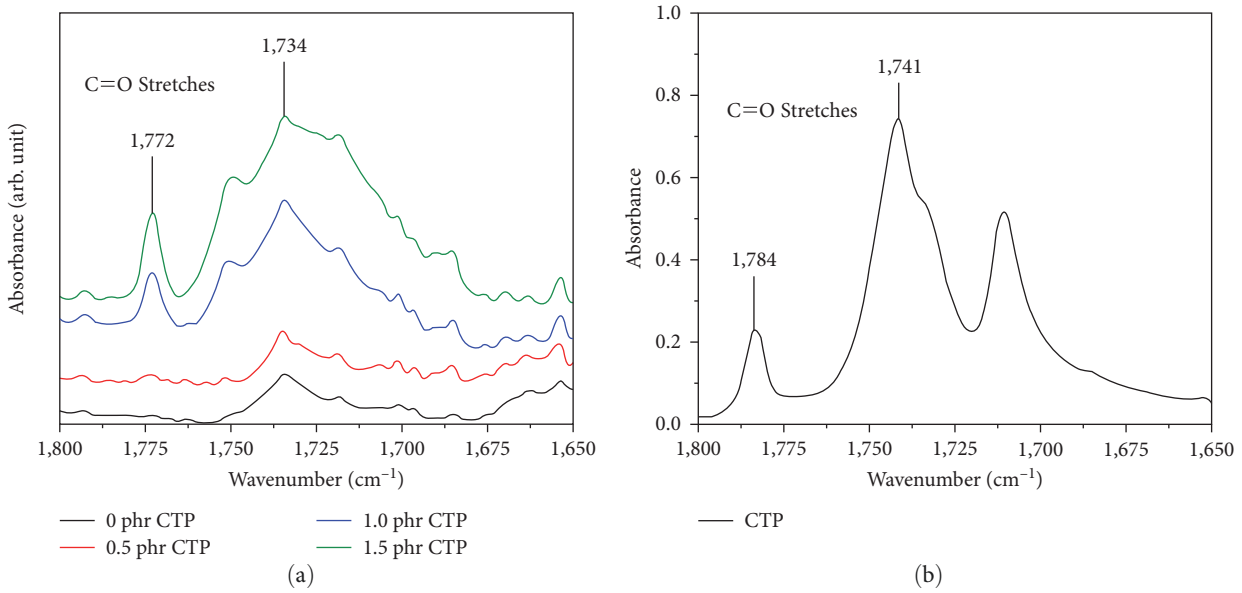

Figure 7: IR-spectra (a) ATR-FTIR spectra of vulcanizates with different CTP contents; (b) IR-transmission spectrum of reference CTP (KBr).

induction period was not extended and strong CTP blooming could be observed from 1.5 phr on. Since the rubber mixture that contained 1 phr CTP showed slight blooming as well, the applications of this sample were restricted to those without exposure to human skin or those used only for prototyping.

3.2.4. Vulcanization Kinetics of NBR–Rubber Mixture #1 with Adjusted Curing System. Another approach is to change the components and the type of curing system fundamentally. In all recipe variations, 3 phr of TBzTD as thiuram derivate was used as a first accelerator to ensure a steep ascent of the rheometer curve and thus fast vulcanization after processing.

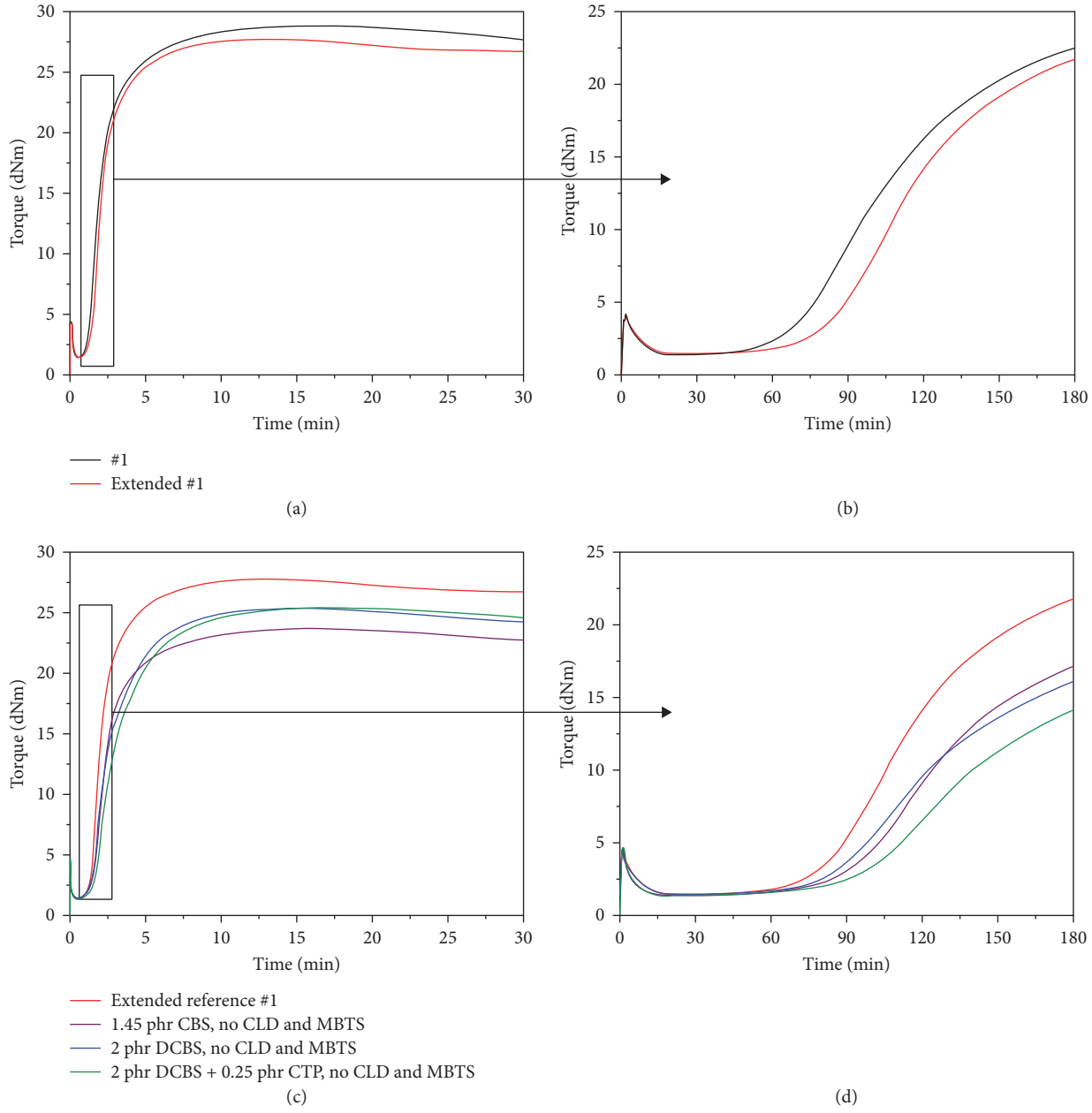

Figure 8: Rheometer curves at 160°C of the optimized rubber recipe #1 (Batch 3) by changing the curing system fundamentally. (a) #1 vs. Extended #1; (b) close up of the induction period of (a); (c) variation of cure components of the recipe including 1 phr stearic acid in all samples and (d) close-up of the induction period of (c).

The concentrations of carbon black, processing agents, antioxidants, zinc oxide and sulfur were kept constant as well to enable a focus on the curing behavior. The sulfur content in these investigations was not varied, so as to retain the ratio of poly-, di- and monosulfide bonds in the network structure as much as possible after the vulcanization. Before the actual crosslinking components were focused on, 1 phr stearic acid was added to the mixture as a common coactivator. The recipe was adopted stepwise, with the aim of achieving an extended scorch time comparable to that achieved by the addition of 1 phr CTP to the mixture, while retaining the mechanical characteristics and crosslinking density of the reference compound #1:

First, the second accelerator, benzothiazole disulfide (MBTS), was omitted to reduce interactions between the numerous accelerators for further test series. The sulfur donator caprolactam disulfide (CLD) was replaced by a double molar of N-Cyclohexylbenzothiazole-2-sulfenamide (CBS) because, unlike CLD as disulfide (sulfur donor), CBS provides only one sulfur atom per molecule. Second, to achieve a higher yield of crosslinks in a slower vulcanization, CBS was exchanged with an equimolar quantity of DCBS in another sample. In a third sample, the second recipe, with DCBS as second accelerator, contained a small additional amount of CTP to extend the induction period while only slightly affecting the mechanical properties. In that way, the induction period could be extended even further

Table 4: Optimization of the curing system: effect of curing system composition on the vulcanization time t_{90}, scorch time t_{10} and maximum torque in the rheometer at 160°C by changing the accelerator type and concentration.

Compound no.	Vulcanization time t_{90} (s)	Scorch time t_{10} (s)	Maximum torque S´ (dNm)
1 (#1, Batch 3)	302	72	28.8
2 (Extended #1 Stearic acid)	277	84	27.8
3 (Stearic acid + CBS)	332	94	23.6
4 (Stearic acid + DCBS)	364	91	25.3
5 (Stearic acid + DCBS + CTP)	409	102	25.4

without decreasing the crosslinking density. The results of the rheometer curves at 160°C are shown in Figure 8.

The numerical values of the vulcanization can be deduced from Table 4.

The rheometer curves of reference compound #1 (black curve) and extended #1 (#1 with 1 phr stearic acid, red curve) are represented in Figures 8(a) and 8(b). The curves show fast vulcanization, followed by a plateau and slow reversion. As the figure indicates, the activating effect of the stearic acid in combination with zinc oxide led to 8% faster vulcanization, whereas the scorch time was extended by 17% (Figure 8). The crosslinking densities of #1 and extended #1 could not be directly compared because of the plasticizing effect of stearic acid, which may have lowered the torque values as well. The rubber mixtures shown in Figure 8(c) and 8(d), which were characterized by their vulcanization behavior, all contained stearic acid. For that reason, the new reference is represented here by the starting recipe with the addition of stearic acid (red curve = extended #1).

The use of 1.45 phr CBS as a second accelerator instead of 1.25 phr CLD and 1.5 phr MBTS lowered the final torque value by 15% (purple curve), indicating a drop in crosslinking density. The scorch time could not be extended further through the replacement of CBS by DCBS; however, the vulcanization time was increased by 31% (blue curve). Due to the longer duration, the crosslinking density was increased, such that the final torque level was 7% higher than with CBS as the second accelerator. Nevertheless, the maximum torque was 12% lower compared to stearic acid extended #1 (red curve). To achieve comparable retardation in the vulcanization kinetics to the use of 1 phr CTP in the mixture (cf. Figure 8), an additional 0.25 phr of CTP was added to the mixture containing DCBS as second accelerator. Through the strong retarding effect of CTP in combination with sulfenamide accelerators, the scorch time could be extended by further 12% without affecting the maximum torque value in the curve. The optimization of the recipe with addition of stearic acid and replacement of MBTS and CLD by DCBS and CTP provided a 42% longer scorch time t_{10} and lowered the maximum torque by 12% compared to starting mixture #1. The direct addition of a higher amount of 1 phr CTP to the mixture extended the scorch time by a comparable 37% and increased the final torque values (11%). Here, the plasticizing effect of the stearic acid did not allow a direct correlation of torque and crosslink density, so tensile tests and swelling experiments were carried out to characterize the mechanical properties and crosslinking density.

3.2.5. Tensile Tests. The mechanical properties of the optimized mixtures in both optimization series were evaluated by tensile tests and compared with reference #1. For that purpose, rubber plates were produced at 160°C in a conventional heat press process at 28 MPa cylinder pressure. The vulcanization time t_{90} for each sample was extended by 2 min compensate for the reduced heat transfer compared to the rheometer. The resulting maximum tensile strength and stress at 50% strain for each content of CTP are shown in Figure 9. The used sample size was $n = 10$.

The maximum tensile strength values were within the range of error for all compounds and slightly higher (17 MPa at 180°C) than those provided by the manufacturer *Schill + Seilacher "Struktol" GmbH* for a fuel resistant sealant compound [34]. The deviation is related to the adaptation of the curing system, the type of filler and polymer, and the difference in vulcanization temperature. However, the median values decreased slightly with an increasing amount of CTP (Figure 9(a)). The stress at 50% strain is a common indicator of the crosslinking density. With an increasing amount of CTP in the mixture, the stress value decreases constantly. In this test, the use of 1 phr CTP produced a reduction of 20%. That behavior was in accordance with the elongation at break, which increased (14%, 1 phr) due to lower crosslinking degree. As the addition of 0.5 phr did not show a significant retardation effect and amounts of CTP from 1.5 phr on led to blooming, the most reasonable amount of CTP was 1 phr, although a drop in the stress at 50% strain values could be observed. Here, the maximum stress of the S2 tensile specimens, as well as the stress at 50% strain of the fundamentally optimized curing systems of rubber mixtures nos. 3–5 in Figure 10, are compared to #1 and stearic acid extended #1 to characterize the influence on mechanical properties. The sample size was $n = 10$.

The maximum strength values of all presented mixtures were in the range of error (Figure 10(a)). The elongation at break value of mixture no. 3 with CBS and stearic acid showed the strongest increase at 12%, probably due to a reduced crosslinking, which was in accordance with the decreased maximum torque values of the rheometer curve (Figure 8(c)). The stress value at 50% strain of mixture 3 was significantly decreased, which confirmed the assumption of an insufficient degree of crosslinking. In mixture no. 5 (also referred to as Recipe #3, see Section 2.1, Table 1), CBS was exchanged for an equimolar amount of DCBS and 0.25 phr CTP was added. The resulting stress at 50% strain was slightly reduced by 6%, but was still in the range of error compared to the reference mixture. When this mixture is

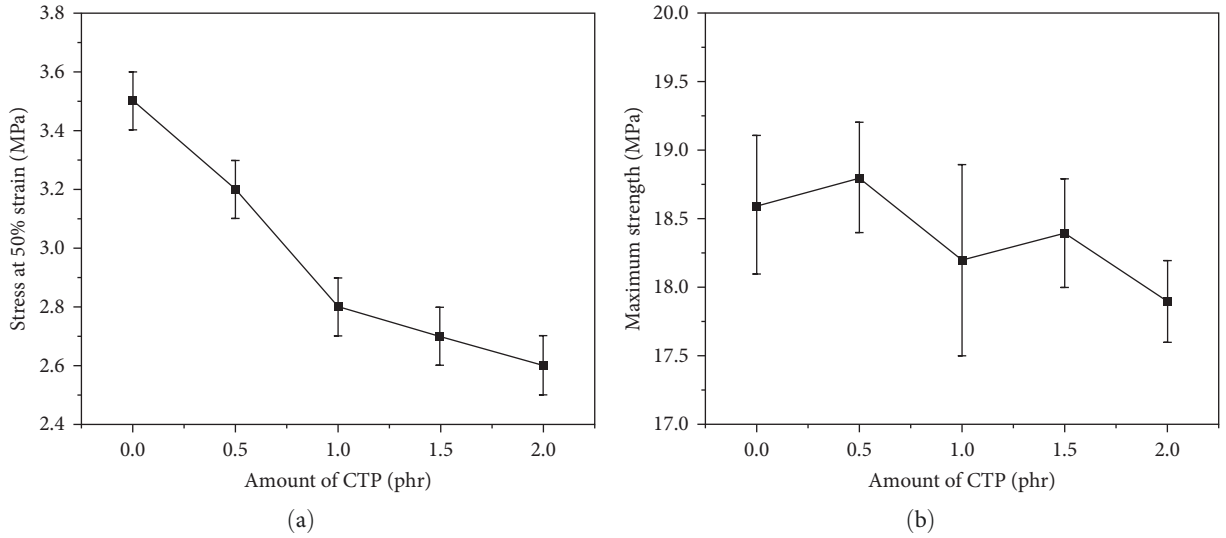

FIGURE 9: Influence of different amounts of CTP on: (a) maximum tensile strength; (b) stress at 50% strain.

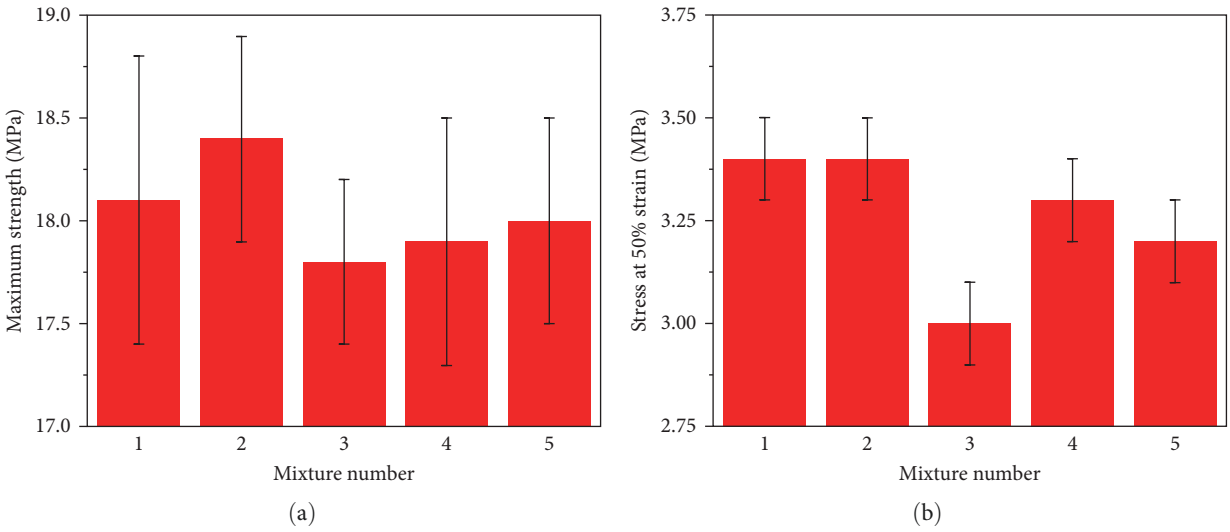

FIGURE 10: Maximum tensile strength of mixtures with optimized curing system (Batch 3): no. 1 : #1; no. 2: extended #1; no. 3: CBS + Stearic acid; no. 4: DCBS + St. Ac.; no. 5: DCBS + CTP + Stearic acid. (a) Maximum tensile strength and (b) stress at 50% strain.

compared to the addition of 1 phr CTP (Figure 9), it is obvious that a fundamental change of curing system is mandatory when the maximum cure and mechanical properties have to retain density for further application.

3.2.6. Rubber Process Analyzer (RPA)—Measurements of Kinetics. The kinetics of the unoptimized (#1) and optimized recipes (#2 and #3) were investigated in detail by means of an RPA to confirm the inhibition of the reaction by an increased activation energy of the optimized compounds. Vulcanization was carried out at three different temperatures (140, 160, 180°C) to determine the activation energy. The calculation of the activation energy E_A is based on the linearized Arrhenius equation:

$$\ln k = \ln A - \frac{E_A}{RT}. \quad (3)$$

The speed constant k is calculated based on the increasing torque in the range of conversion of 10%–90% based on the maximum torque during vulcanization for each temperature T. The activation energy is obtained by linear regression using the rate constants at three different temperatures, where the slope is $-E_A \cdot R^{-1}$ with the ideal gas constant R. The intersection with the Y-axis represents the logarithmic preexponential factor A, which represents the frequency to overcome the activation energy in the reaction [35]. The numerical values of the activation energies and the rate constants at different temperatures are compared in Table 5.

From Table 5, can be deduced that additional 1 phr CTP (Sample #2, Batch 2) increased the activation energy for the vulcanization by 9%, while the fundamental optimization with the use of DCBS as a binary accelerator and 0.25 CTP (Sample #3, Batch 3) as PVI increased it by 14%. The rate

Table 5: Activation energy and rate constant of unoptimized and optimized recipes.

Recipe	Activation energy E_A (kJ·mol^{-1})	Speed constant k at 160°C (min^{-1})	Coefficient of determination R^2
#1: Reference	72.0	−1.58	0.993
#2: Optimized with 1 phr CTP	78.6	−0.97	0.996
#3: Optimized by exchanging the curing system	82.4	−0.62	1.000

constant of both optimized samples decreased (−39%, Sample #2; −61%, Sample #3).

3.2.7. Swelling. To determine the crosslink density of the compounds, swelling experiments with tetrahydrofuran (THF) for 24 hr at room temperature were carried out. Swelling is a widely used approach to determine the cross-linking density of elastomers, but with uncertainties in the results [36]. Since the crosslinking reaction occurs inhomogeneously throughout the sample, this method gives the average crosslinking density over the volume of the sample and thus can be considered as a qualitative method to provide a comparison of the samples. In addition, THF can dissolve extractables of the compounds and thus interfere with the results. The mass uptake of solvent in such experiments correlates with the crosslink density D_c and can be calculated by the Flory–Rehner equation [37]:

$$D_c = \frac{v_{NBR} + \chi v_{NBR}^2 + \ln(1 - v_{NBR})}{-v_{THF}\left(\sqrt[3]{v_{NBR}} - \frac{v_{NBR}}{2}\right)} \quad (4)$$

Here, χ is the Flory–Huggins interaction parameter between THF and NBR, v_{THF} is the molar volume of THF (81 cm^3·mol^{-1}) and v_{NBR} is the volume ratio of the swollen NBR sample. The latter is given by

$$v_{NBR} = \frac{m_{NBR}}{m_{NBR} + m_{THF}\left(\frac{\rho_{NBR}}{\rho_{THF}}\right)}, \quad (5)$$

where m_r is the mass of the rubber network, m_s is the mass of the solvent in equilibrium state, and ρ_r and ρ_{is} the respective densities of rubber and the solvent. In this case, the interaction parameter χ was calculated from the Hansen solubility parameters of THF [38] $\delta_{THF} = 9.49$ (cal·cm^{-3})$^{0.5}$ and NBR [39] with 33% acrylonitrile content $\delta_{NBR33} = 9.57$ (cal·cm^{-3})$^{0.5}$ by using the following equation [40, 41]:

$$\chi = 0.35 + \frac{v_{THF}}{RT}(\delta_{THF} - \delta_{NBR33})^2 \quad (6)$$

The calculated crosslink density of the reference mixture (#1, Batch 4) and both optimized mixtures (recipes #2 and #3, Batch 4) are compared in Figure 11.

In these investigations, only the number of crosslinks was investigated; the relation between mono-, di- and polysulfide bonds was not considered. Moreover, the Flory-Rehner approach is valid for unfilled compounds. The calculated crosslink densities for the carbon black content were not corrected, and thus they could not be regarded as absolute values.

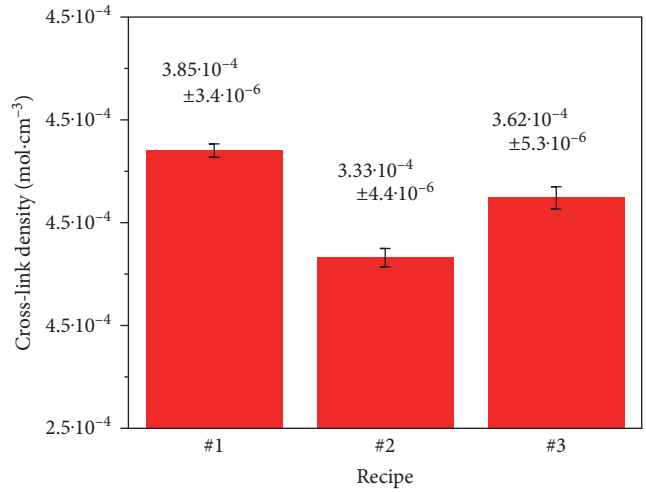

Figure 11: Comparison of the crosslink densities of the reference (recipe #1) and both optimized mixture vulcanizates (recipe #2 and #3), as determined by swelling in THF at 25°C for 24 hr. The number of samples each recipe was $n = 3$.

Nevertheless, relative comparison was possible, because the content of carbon black was equal and the same dispersion can be assumed in all compounds. The order of magnitude of the calculated crosslink densities were consistent with those reported in the literature for NBR rubber elastomers [42]. Both optimized recipes showed decreased crosslink densities compared to the reference samples. Recipe #2 contained the highest amount of CTP at 1 phr, lowering the crosslink density by 13%. Recipe #3 showed a reduction of 6% compared to the reference recipe #1, although the extension of the scorch period was comparable that in to recipe #2.

3.2.8. Mooney Scorch and Additive Manufacturing of the O-Ring. Before the actual additive manufacturing of the components were carried out, Mooney scorch measurements were used to pre-estimate the scorch behavior at 100°C printing temperature in the extruder during printing. Thus, the required material for the NBR-based O-ring was 1.4 g and the stored material in the extruder was 4.5 g. No complete material exchange could take place while printing one single part, so the scorch safety has to be ensured over the entire printing time of the 2K part, and preferably more, for more safety in the process. In this study, using printing velocities of 20 and 10 mm·s^{-1} for TPU and rubber,

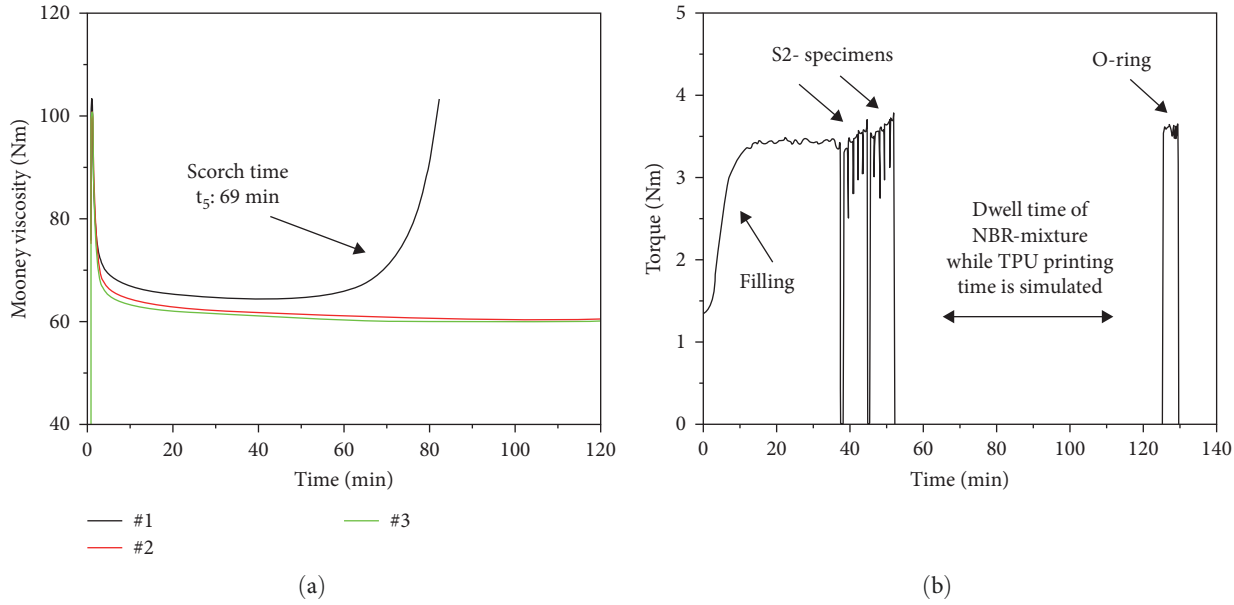

FIGURE 12: Pre-estimation of scorch behavior of the rubber mixtures and 3D printing. (a) Mooney Scorch measurements of the reference mixture (#1, Batch 4) and both optimized mixtures (#2, #3, Batch 4) at 100°C, (b) torque curve during the 3D printing at 100°C.

FIGURE 13: Additive manufacturing of the rod seal. (a) Geometrically shaped design of the O-ring, (b) printed O-ring, (c) assembled seal of both additively manufactured parts, and (d) conventional rod seal with X-shaped O-ring.

repectively, resulted in a total time of 70 min (1 : 06 hr TPU; 4 min NBR) for the 2K part. The scorch behavior of the reference mixture (#1; Batch 4) and both optimized mixtures (#2, #3; Batch 4) is characterized and compared in Figure 12(a). The torque curve during subsequent 3D printing of the O-ring (recipe #3) is represented in Figure 12(b).

The scorch time t_5 of reference mixture (recipe #1) was 69 min, which was insufficient to carry out 3D printing with the 2K part. Neither recipe #2 nor recipe #3 showed scorching within 120 min. The compound with the exchanged curing system (recipe #3) was used in subsequent 3D printing. From Figure 12, it can be deduced that the initial filling of the extruder by feeding with 2 mm NBR rubber stripes was accompanied by an increase in torque up to equilibrium conditions from 15 min on. When extrusion is carried out in 3D printing, the short nozzle distance to the printing bed increases the pressure and thus the torque and throughput raises. In this instance, two S2 tensile test specimens were printed to again achieve an equilibrium of torque, and thus throughput. Their weight was determined (specimen #1 : 2.1 g, specimen #2 : 2.3 g) to ensure comparable printing conditions in all printing experiments. Before the actual O-ring was manufactured, the printing time of the TPU was simulated (1 hr 10 min), leading to a dwell time of the NBR-based rubber mixture in the extruder. The torque level while printing the O-ring was comparable to those of the second printed S2 test specimens, and it remained constant during the entire manufacturing period. Due to an insufficient printing resolution with the 0.6 mm nozzle diameter, the CAD model of the O-ring had to be simplified to a rectangular shape to achieve a printable geometry, as shown in Figure 13(a). The fine structures of the X-shape would also require a thermoplastic support structure that could not be removed if the entire seal was printed in one step in a future stage. The completed O-ring, the assembled part and the conventional seal are depicted in Figure 13(b)–13(d), respectively. The printed TPU was manufactured using the filament type *Extrudr* Semisoft A88 [43].

The O-ring could be printed successfully after the dwell time at 100°C in the extruder with a smooth homogeneous surface. The starting point of each layer was located at the same position, leading to accumulated material in one part of the O-ring (Figure 13(b)). After assembling the rod seal

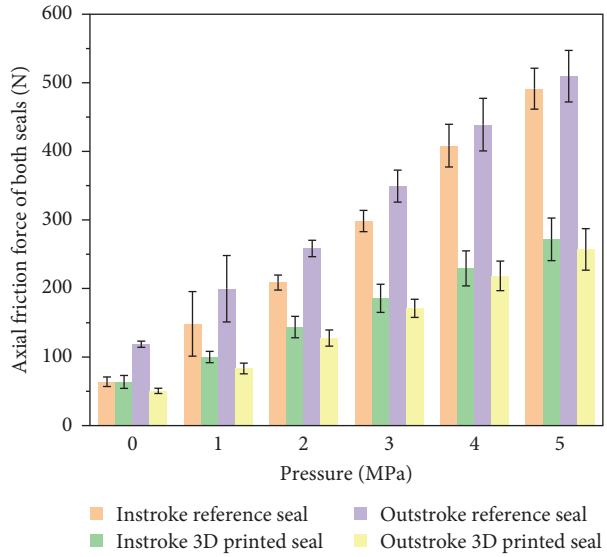

Figure 14: Axial friction force of seals respective different pressure levels. The reference seal on the right-hand side was always mounted. This means the measured values in this graph included the axial friction forces of both seals (sample size $n = 3$).

Table 6: Numerical values of tensile tests of S2 specimens (from 3D-printing, recipe #3, Batch 3) after vulcanization at 160°C are compared with the results of conventional heat press.

Sample/test direction	Maximum strength (MPa)	Elongation at break (%)	Stress at 50% strain (MPa)
Heated press (conventional)	18.0 ± 0.5	261.4 ± 16.6	3.2 ± 0.1
0° to printing direction	16.0 ± 0.3	282.1 ± 14.1	2.2 ± 0.1
90° to printing direction	9.2 ± 1.0	167.7 ± 15.2	2.0 ± 0.1

The data are based on the median values of a test series each of $n = 10$.

(Figure 13(c)), the part was vulcanized in an oven. In Figure 13(d), the conventional rod seal is demonstrated.

3.2.9. Tensile Tests of Additively Manufactured Parts. To evaluate the mechanical properties of the additively manufactured part, which was based on recipe #3, it was printed with the same process parameters that were used for manufacturing the rod seal. For the characterization, S2 tensile test specimens were punched out from an additively manufactured and vulcanized rubber mat of different printing patterns. The vulcanization time t_{90} of the used mixture had to be extended by 8 min to obtain the final vulcanization time t_{final} of 14 min 48 s according to experimentally supported simulation (see Equation (2) and Table 4). The numerical values of the results of the tensile test are represented in Table 6.

The test specimens, which were tested 0° to the printing direction, provided a maximum strength of 16 MPa, which amounted to a 12% decrease compared to the part manufactured in the heated press. This can be attributed to the fact that maintaining an angle of 0° was difficult to achieve manually while punching out the samples, so that slight shifts in the angle could have led to a reduce number of continuous rubber stripes in the specimen's test area. After manufacturing of the heat pressed samples, punching out takes place as well, but in this case the angle shift can be neglected, because the sample does not consist of multiple stipes, which from this point of view give a relatively isotropic material character. For both manufacturing methods cutting out of the specimens causes a deformation of the cross-sectional area to a trapezium shape of the specimen, that leads to a deviation from the true stress values. Especially, the true cross-section of the additively manufactured specimen is influences additionally by the wavy like surface. The description of theses phenomena and an approach for the correction was reported by Oelsch et al. [44]. Furthermore, the additive manufacturing process may have created small voids due to an uneven manufacturing process [4], which can be considered defects that could initiate rupture. The elongation at break was extended by 17% and the stress at 50% strain was lowered by 30%, which may indicate a slight undervulcanization. The height of the rubber mats in the CAD model was 2 mm, resulting in six layers. However, the over-extrusion in the additive manufacturing enlarged the dimensions in z-direction. The resulting increased thickness of more than 50% was not considered in the pre-estimated final vulcanization time t_{final} in the oven. The mechanical stability of 90° to the printing direction was, as expected, strongly decreased due to the created interfaces between rubber stripes, leading to a reduced connection. In addition, the wavy structure of the surface due to the manufacturing process could be seen as numerous notches [44], which could also have been responsible for an initiation rupture.

3.3. Functionality Tests of the Additively Manufactured Seal. The rod seal test stand at the University of Applied Sciences in Emden was used to evaluate whether the first specimens were working. These first tests also included the measurement of the axial friction force, but were mainly meant as a qualitative analysis to check the compliance with the main function (i.e., avoiding the leakage of hydraulic fluid). In the event of a failure, the pump must be shut down to prevent further contamination of the area. For this reason, the seal at the pump site is the commercially available reference seal, which allows safe operator access to the pump. The reference seal is suitable for a large number of experiments without showing significant changes in sealing characteristics, so that the same seal remained at the pump site for all experiments. Changes in the measured axial forces can thus be attributed to the additively manufactured test part. Figure 14 shows the axial forces of the first test seals compared to the reference measurement.

It could be demonstrated that 3D-printed seals served their main function: no leakage occurred. The lower axial forces of the additively manufactured rod seals may be due to softer material or different deformation behavior, resulting in lower radial force and therefore lower axial force in dynamic tests. Although less power is dissipated, this is not a problem as long as the primary sealing function is met. However, the stagnation of the force increase with increasing pressure could be a signal that at a certain increased pressure, leakage would occur sooner than with the reference seal. Another explanation for the reduced axial forces is the increased fluid supply in the contact zone between the seal and the rod, especially at lower speeds, due to the different rough surface structure of the 3D printed parts. Thus, the seal is not completely symmetric, differences in radial forces between conventional and 3D printed samples can lead to deviations in the in and out stroke values. In order to assign the exact contribution of each seal to the in and out stroke values, a test setup must be found in which a single seal can be characterized.

4. Conclusions

It could be demonstrated that additive manufacturing of a rod seal was realized with a conventional rubber mixture. In the printing process of the 2K seal, the waiting period when the TPU component was manufactured had to be overcome without any scorching. For that purpose, the curing kinetics were extended by enhancing the activation energy of the cross-linking. Mooney Scorch measurements indicated that both optimization strategies extended the scorch time sufficiently to use the relevant compound in 3D printing. However, the easy approach with the addition of 1 phr CTP to the compound resulted in a reduced cure density, which could be confirmed by swelling experiments and tensile tests. Nevertheless, it is a rational first approach that does not require human exposure for prototyping or estimation of first manufacturing results when there is little mechanical stability and chemical resistance gains importance in final applications. The cure system must be adopted, as was exemplarily demonstrated in this work. The role of simulation as an essential pre-estimation method for vulcanizing 3D-printed parts was validated by the fact that the drop in temperature after opening the door of the oven caused a deviation from the experimentally determined vulcanization time. That has to be considered in future simulations.

Data Availability

The data used to support the findings of this study are available from the corresponding author upon request.

Conflicts of Interest

The authors declare that they have no conflicts of interest.

Acknowledgments

The work was funded by the Deutsche Forschungsgemeinschaft (DFG) (project no. 447009134). Open Access funding enabled and organized by Projekt DEAL.

References

[1] J. Stieghorst, D. Majaura, H. Wevering, and T. Doll, "Toward 3D printing of medical implants: reduced lateral droplet spreading of silicone rubber under intense IR curing," *ACS Applied Materials & Interfaces*, vol. 8, no. 12, pp. 8239–8246, 2016.

[2] F. Asai, T. Seki, A. Sugawara-Narutaki et al., "Tough and three-dimensional-printable Poly(2-methoxyethyl acrylate)–silica composite elastomer with antiplatelet adhesion property," *ACS Applied Materials & Interfaces*, vol. 12, no. 41, pp. 46621–46628, 2020.

[3] L. Sundermann, S. Leineweber, B. Klie, U. Giese, and L. Overmeyer, "Development, construction and testing of a 3D-printing-system for additive manufacturing of carbon black filled rubber compounds," *KGK Kautschuk Gummi Kunststoffe*, vol. 73, Article ID 30, 2020.

[4] S. Leineweber, L. Sundermann, L. Bindszus et al., "Additive manufacturing and vulcanization of carbon black–filled natural rubber–based components," *Rubber Chemistry and Technology*, vol. 95, no. 1, pp. 46–57, 2022.

[5] S. Leineweber, B. Reitz, L. Overmeyer, L. Sundermann, B. Klie, and U. Giese, "Additive manufacturing and vulcanization of natural and synthetic rubbers," *Logistics Journal: Proceedings*, pp. 1–9, 2022.

[6] L. Sundermann, B. Klie, U. Giese, K. Ottink, and M. Graf, "Additive manufacturing of 2-component rod seals based on nitrile butadiene rubber (NBR) and thermoplastic polyurethanes (TPU)," in *presented on 2nd Global Summit on 3D Printing & Additive Manufacturing*, p. 17, published by O. Gülcan, Copenhagen, Denmark, 2022.

[7] W.-G. Drossel, J. Ihlemann, R. Landgraf, E. Oelsch, and M. Schmidt, "Basic research for additive manufacturing of rubber," *Polymers*, vol. 12, no. 10, Article ID 2266, 2020.

[8] W.-G. Drossel, J. Ihlemann, R. Landgraf, E. Oelsch, and M. Schmidt, "Media for dimensional stabilization of rubber compounds during additive manufacturing and vulcanization," *Materials*, vol. 14, no. 6, Article ID 1337, 2021.

[9] S. H. Khajavi, J. Partanen, and J. Holmström, "Additive manufacturing in the spare parts supply chain," *Computers in Industry*, vol. 65, no. 1, pp. 50–63, 2014.

[10] H. Wittek, B. Klie, U. Giese, S. Kleinert, L. Bindszus, and L. Overmeyer, "Approach for additive manufacturing of high-viscosity, curable rubbers by AME processing (Additive Manufacturing of Elastomers) – Rubber 3D," *KGK Kautschuk Gummi Kunststoffe*, vol. 72, pp. 53–56, 2019.

[11] M. Graf, T. Ebel, T. Lankenau, and K. Ottink, "Towards additively manufactured dynamic rod seals," in *21st ISC*, pp. 47–62, Fachverband Fluidtechnik im VDMA e.V., Stuttgart, 2022.

[12] G. R. Hamed and T. Donatelli, "Effect of accelerator type on brass-rubber adhesion," *Rubber Chemistry and Technology*, vol. 56, no. 2, pp. 450–464, 1983.

[13] S. O. Movahed, A. Ansarifar, and F. Mirzaie, "Effect of various efficient vulcanization cure systems on the compression set of a nitrile rubber filled with different fillers," *Journal of Applied Polymer Science*, vol. 132, no. 8, Article ID 41512, 2015.

[14] B. Saville and A. A. Watson, "Structural characterization of sulfur-vulcanized rubber networks," *Rubber Chemistry and Technology*, vol. 40, no. 1, pp. 100–148, 1967.

[15] A. Y. Coran, "Vulcanization. Part IV. The effects of compounding variables on the nature of rubber networks," *Rubber Chemistry and Technology*, vol. 37, no. 3, pp. 673–678, 1964.

[16] E. Morita and E. J. Young, "A study of sulfenamide acceleration," *Rubber Chemistry and Technology*, vol. 36, no. 3, pp. 844–862, 1963.

[17] A. M. Joseph, B. George, K. N. Madhusoodanan, and R. Alex, "Current status of sulphur vulcanization and devulcanization chemistry: Process of vulcanization," *Rubber Science*, vol. 28, pp. 82–121, 2015.

[18] A. Y. Coran, C. D. Trivette Jr., and J. E. Kerwood, (Monsanto Co.), US3546185A, 1970.

[19] M. H. S. Gradwell and N. R. Stephenson, "Pre-vulcanization inhibition of a N-t-butyl-2-benzothiazole sulfenamide cure by N-(cyclohexylthio)phthalimide," *Rubber Chemistry and Technology*, vol. 77, no. 5, pp. 931–946, 2004.

[20] R. I. Leib, A. B. Sullivan, and C. D. Trivette Jr., "Prevulcanization inhibitor the chemistry of scorch delay," *Rubber Chemistry and Technology*, vol. 43, no. 5, pp. 1188–1193, 1970.

[21] P. N. Son, "Some observations on the mechanism of cure retardation," *Rubber Chemistry and Technology*, vol. 46, no. 4, pp. 999–1006, 1973.

[22] R. Mukhopadhyay and S. K. De, "Effect of curing systems and temperatures on the activity of retarder in natural rubber mixes," *Polymer*, vol. 20, no. 12, pp. 1527–1530, 1979.

[23] S. Mostoni, P. Milana, B. Di Credico, M. D'Arienzo, and R. Scotti, "Zinc-based curing activators: new trends for reducing zinc content in rubber vulcanization process," *Catalysts*, vol. 9, no. 8, Article ID 664, 2019.

[24] G. Heideman, R. N. Datta, J. W. M. Noordermeer, and B. van Baarle, "Influence of zinc oxide during different stages of sulfur vulcanization. Elucidated by model compound studies," *Journal of Applied Polymer Science*, vol. 95, no. 6, pp. 1388–1404, 2005.

[25] C. R. Parks, D. K. Parker, D. A. Chapman, and W. L. Cox, "Pendent accelerator groups in rubber vulcanizates," *Rubber Chemistry and Technology*, vol. 43, no. 3, pp. 572–587, 1970.

[26] P. Junkong, R. Morimoto, K. Miyaji, A. Tohsan, Y. Sakaki, and Y. Ikeda, "Effect of fatty acids on the accelerated sulfur vulcanization of rubber by active zinc/carboxylate complexes," *RSC Advances*, vol. 10, no. 8, pp. 4772–4785, 2020.

[27] M. M. Coleman, J. Reid Shelton, and J. L. Koenig, "Sulfur vulcanization of hydrocarbon diene elastomers," *Industrial & Engineering Chemistry Product Research and Development*, vol. 13, no. 3, pp. 154–166, 1974.

[28] F. Röthemeyer and F. Sommer, *Kautschuk Technologie*, Hanser, München, 2013.

[29] K. T. Gillen and R. L. Clough, "Rigorous experimental confirmation of a theoretical model for diffusion-limited oxidation," *Polymer*, vol. 33, no. 20, pp. 4358–4365, 1992.

[30] K. T. Gillen, R. Bernstein, and M. Celina, "Challenges of accelerated aging techniques for elastomer lifetime predictions," *Rubber Chemistry and Technology*, vol. 88, no. 1, pp. 1–27, 2015.

[31] U. Giese, S. Kautz, C. Schwarzendahl, and S. Thust, "Degradation of Elastomers in Practice, Experiments and Modeling," in *Advances in Polymer Science*, G. Heinrich, R. Kipscholl, and R. Stoček, Eds., vol. 289, pp. 317–344, Springer, Cham, 2023.

[32] F. Saeed, A. Ansarifar, R. J. Ellis, Y. Haile-Meskel, and A. S. Farid, "Effect of the blooming of chemical curatives on the cyclic fatigue life of natural rubber filled with a silanized silica nanofiller," *Journal of Applied Polymer Science*, vol. 120, no. 5, pp. 2497–2507, 2011.

[33] B. C. Smith, "Organic nitrogen compounds VIII: imides," *Spectroscopy*, vol. 35, no. 3, pp. 26–30, 2020.

[34] Schill+Seilacher, *Struktol-Compounding Guide*, vol. 22, p. 22, 2017, https://struktol.de/de/downloads/kautschuk/.

[35] P. P. Richard Hanzlik, "Most effective viscoelastic properties from the rubber process analyzer for measuring factory quality of mix," *Rubber and Plastics News*, pp. 13–17, 2021.

[36] J. L. Valentín, J. Carretero-González, I. Mora-Barrantes, W. Chassé, and K. Saalwächter, "Uncertainties in the determination of cross-link density by equilibrium swelling experiments in natural rubber," *Macromolecules*, vol. 41, no. 13, pp. 4717–4729, 2008.

[37] Z. Xia, M. Patchan, J. Maranchi, J. Elisseeff, and M. Trexler, "Determination of crosslinking density of hydrogels prepared from microcrystalline cellulose," *Journal of Applied Polymer Science*, vol. 127, no. 6, pp. 4537–4541, 2013.

[38] J. Brandrup, E. H. Immergut, and E. A. Grulke, *Polymer Handbook*, Wiley, New York, 4th edition, 1999.

[39] G. N. Campos, A. C. R. Coimbra, A. A. Da Silva et al., "Cross-link density measurement of nitrile rubber vulcanizates using dynamic shear testa," *Polímeros*, vol. 32, no. 1, Article ID e2022011, 2022.

[40] A. J. Marzocca, A. L. Rodríguez Garraza, and M. A. Mansilla, "Evaluation of the polymer–solvent interaction parameter χ for the system cured polybutadiene rubber and toluene," *Polymer Testing*, vol. 29, no. 1, pp. 119–126, 2010.

[41] D. Y. Kim, J. W. Park, D. Y. Lee, and K. H. Seo, "Correlation between the crosslink characteristics and mechanical properties of natural rubber compound via accelerators and reinforcement," *Polymers*, vol. 12, no. 9, 2020.

[42] S. N. Lawandy and S. F. Halim, "Effect of vulcanizing system on the crosslink density of nitrile rubber compounds," *Journal of Applied Polymer Science*, vol. 96, no. 6, pp. 2440–2445, 2005.

[43] FD3D GmbH, Technical data sheet, TPU Flex Semisoft, 2022.

[44] E. Oelsch, R. Landgraf, L. Jankowsky et al., "Comparative investigation on the mechanical behavior of injection molded and 3D-printed thermoplastic polyurethane," *Journal of Rubber Research*, vol. 24, pp. 249–256, 2021.